International Journal of Modern Physics E
Vol. 25, No. 6 (2016) 1650034 (21 pages)

DOI: 10.1142/S0218301316500348

World Scientific
www.worldscientific.com

Sensibility of grey particle production system to energy and centrality in 60 A and 200 A GeV ^{16}O–Nucleus interactions

A. Abdelsalam[*,§], M. S. El–Nagdy[†,§], B. M. Badawy[‡,§,¶], W. Osman[*,§] and M. Fayed[*,§]

[*]*Physics Department, Faculty of Science, Cairo University, Giza, Egypt*

[†]*Physics Department, Faculty of Science, Helwan University, Helwan, Egypt*

[‡]*Reactor Physics Department, Nuclear Research Center, Atomic Energy Authority, Egypt*

[§]*Mohamed El–Nadi High Energy Laboratory, Faculty of Science, Cairo University, Egypt*

[¶]*he_cairo@yahoo.com*

Received 8 September 2015
Revised 14 April 2016
Accepted 26 April 2016
Published 1 June 2016

The grey particle production following 60 A and 200 A GeV ^{16}O interactions with emulsion nuclei is investigated at different centralities. The evaporated target fragment multiplicity is voted as a centrality parameter. The target size effect is examined over a wide range, where the C, N and O nuclei present the light target group while the Br and Ag nuclei are the heavy group. In the framework of the nuclear limiting fragmentation hypothesis, the grey particle multiplicity characteristics depend only on the target size and centrality while the projectile size and energy are not effective. The grey particle is suggested to be a multisource production system. The emission direction in the 4π space depends upon the production source. Either the exponential decay or the Poisson's peaking curves are the usual characteristic shapes of the grey particle multiplicity distributions. The decay shape is suggested to be a characteristic feature of the source singularity while the peaking shape is a multisource super-position. The sensibility to the centrality varies from a source to other. The distribution shape is identified at each centrality region according to the associated source contribution. In general, the multiplicity characteristics seem to be limited w.r.t. the collision system centrality using light target nuclei. The selection of the black particle multiplicity as a centrality parameter is successful through the collision with the heavy target nuclei. In the collision with the light target nuclei it may be qualitatively better to vote another centrality parameter.

[¶]Corresponding author.

Keywords: Grey particle multiplicity; dependence on target size; dependence on centrality; emission characteristics; nuclear limiting fragmentation.

PACS Number(s): 25.75.−q, 25.75.Dw, 25.75.Gz, 25.75.Ld, 25.70.Mn, 25.70.Pq, 41.75.Ak, 41.75.Cn, 29.40.Rg, 07.68.+m

1. Introduction

In the photographic nuclear emulsion, the target fragments are identified as grey and black particle tracks.[1,2] The grey particles are, mainly, fast target protons.[3] In interactions with emulsion nuclei at 2.1 A up to 200 A GeV, Otterlund *et al.*[4] attribute the distribution of protons with energy of 30–400 MeV to the grey track producing particles. In the interactions of 14.6 A up to 200 A GeV ^{16}O with emulsion nuclei, Adamovich *et al.*[5] define the target associated particles, mainly, as knocked out protons and evaporated fragments from the target. In general, the grey particles are considered fast protons emitted in the early stage of the target fragmentation. Then, the slow protons are evaporated from the target nuclei in a later stage, the so called black particles. On the basis of the modified Maxwell–Boltzmann distribution, Heckman *et al.*[6] derive the so-called statistical model to predict the system of the slow proton emission. Therefore, this system is thermalized. Abdelsalam[7] suggests that the grey particles may be emitted from a thermalized system also. The emission system temperatures of the grey and black particles are predicted in the framework of the modified statistical model as 60 MeV and 6 MeV, respectively.[7,8] Therefore, the grey particles are sourced from a hot nuclear matter. The black particles are evaporated easily by acquiring energy just equals to the binding energy per nucleon.[7,8] From a kinematic point of view, the backward particle emission is restricted. Hence, this emission is considered beyond the kinematic limits. In this species, experimental efforts are carried out in Lawrence Berkeley National Laboratory, LBNL.[9–11] In 2.1 GeV pA collisions, about 50% of events are associated by negative tracks emission. They can be identified as pions. These pions are distributed in the forward hemisphere, FHS, at $\theta_{\rm lab} < 90^\circ$. The observed tracks in the backward hemisphere, BHS, at $\theta_{\rm lab} \geq 90^\circ$ are typically defined as protons. Thus, the backward proton emission is often accompanied by a Pion emission. Harris[12] suggests two possibilities for the backward proton emission. The first is a pion production followed by its absorption on two target nucleons resulting in two back-to-back nucleons emission. The second is a production of Δ which is absorbed, subsequently, by a target nucleon, $\Delta N \rightarrow NN$, resulting in two protons emission of 180° correlation angle nearly. On the other hand, the limiting fragmentation hypothesis is introduced by Benecke *et al.* in high-energy hadron–hadron, hh, collisions.[13] In LBNL experiment, the onset of the nuclear limiting fragmentation, NLF, is nearly found at $E_{\rm lab} \geq 1$A GeV.[14] Accordingly, a few A GeV energy domain, (say Dubna and Bevalac energies), can be considered the onset of the NLF.[15–17] EMU01 collaboration[4,5] observe that the NLF is fulfilled

in the energy range ($E_{\rm lab} = 14$ A up to 200 A GeV). In the framework of the dual parton model, Brogueira *et al.*[18] examine the validity of the NLF at LHC energy ($\sqrt{S}_{NN} = 5500$ GeV). In Brookhaven National Laboratory, BNL, PHOBOS and BRAHMS collaborations rediscover also the NLF.[19–23]

The fixed target experiments are guidelines in simulating the nuclear destruction applications equipments in practical life. Recently, Abdelsalam *et al.*[24] examined the energy and system size effects on the grey particle production system in 60 A and 200 A GeV ^{16}O interactions with emulsion nuclei. A sample of inelastic interactions is voted with no biasing to any centrality criterion. In the present work, the grey particle production system is examined under the effects of the energy, centrality, target size, and emission direction using the same interactions.

2. Experiment Technique

2.1. *Interaction characteristics*

In EMU03 CERN experiment, the FUJI and ILFORD–G5 nuclear emulsion stacks are irradiated by 60 A and 200 A GeV ^{16}O ion beams, respectively, at the SPS. Each pellicle of the FUJI emulsion type has 12 cm × 4 cm × 0.07 cm size. The pellicle is coated on both sides by polystyrene films. The thickness of each film is 0.007 cm. The ILFORD–G5 emulsion type pellicle has dimensions of 15 cm × 6 cm × 0.06 cm. This emulsion is low sensitive to the lightly-ionizing particle tracks as those flying with relativistic velocity. Accordingly the identification of the relativistic hadron is difficult. The chemical composition of the used emulsion types is displayed in Table 1. The densities are given in (atoms × 10^{22}/cm^3).

The emulsion pellicles' scanning is carried out using 850050 STEINDORFF German microscopes. It has a stage of 18 cm × 16 cm^2 with an opening 7.0 cm × 2.5 cm^2. Stage adjustment in the x-direction is possible over a total length 7.8 cm with reading accuracy of the order of 0.1 mm. Oil immersion objective lens with magnification 100X is used for scanning the emulsion plates. Starting close to the entrance of the beam double scanning is carried out, going into the emulsion 0.5 cm ("fast" in the forward direction and "slow" in the backward direction). Each primary track is picked up at the penetrating edge of the pellicle and is followed forward optically until it either interacts or escapes from the pellicles. The total scanned lengths, L, of the present beams, the associated number of inelastic interactions, N, and the corresponding average mean free path, λ, are listed in Table 2. The mean free path is determined as; $\lambda = L/N$. The simulated mean free paths according to the

Table 1. The chemical composition of the used emulsion types.

Element	^{1}H	^{12}C	^{14}N	^{16}O	^{32}S	^{80}Br	^{108}Ag	^{133}I
FUJI	3.2093	1.3799	0.3154	0.9462	0.0134	1.0034	1.0093	0.0055
ILFORD G5	3.1900	1.3900	0.3200	0.9400	0.0140	1.0100	1.0200	0.0060

Table 2. ^{16}O beams data.

$E_{\rm lab}$	$L_{\rm m}$	N events	λ cm	Emulsion type	Ref.
60 A GeV	130.6	997	13.10 ± 0.40 (10.71)	FUJI	Present work
200 A GeV	103.5	802	12.90 ± 0.50 (10.68)	ILFORD G5	
200 A GeV	—	—	12.30 ± 0.30	BR–2	26
3.7 A GeV	357.689	2960	12.08 ± 0.22	NIKFI BR–2	27

Glauber's approach [25] are listed in Table 2 within round brackets. Table 2 also gives measured values from other labs.

2.2. *Target separation*

The nuclear emulsion is a homogeneous mixture of nuclei with densities corresponding to those given in Table 1. The target size is usually examined by discriminating the total sample of events into groups, in which adequate statistics are enclosed. They are corresponding to H nuclei, CNO (the light target size), and AgBr (the heavy target size). The effective masses of these targets are 1, 14 and 94, respectively. There are several methods to determine the percentage probabilities, $P_{\rm H}$, $P_{\rm CNO}$ and $P_{\rm AgBr}$, belonging to fractions of H, CNO and AgBr target nuclei, respectively.[28–31] In this experiment, the percentages are simulated theoretically using the Glauber's approach encoded in Ref. 25. They are 10.5%, 34.5% and 55% according to H, CNO and AgBr, respectively. These percentages are nearly equivalent to 105, 344 and 548 events, respectively at 60 A GeV. In the same respect, they are 84, 277 and 441 events, at 200 A GeV. The heavily ionizing particle multiplicity, N_h, is the fundamental parameter used in the separation. This parameter indicates the fragmented target nuclear charge. The statistical sample belonging to H locates at $N_h \leq 1$, where its atomic no. is 1. The CNO nuclei events are enclosed in the interval of $0 \leq N_h \leq 8$, where the highest atomic no. is 8. The AgBr sample can have $0 \leq N_h \leq 47$, where the higher atomic no. is 47. Any event having $N_h > 8$ is purely due to a collision with AgBr while these at $N_h \leq 8$ are contributed by collisions with H, CNO, or AgBr. For simplicity, let us apply this separation on the data belonging to any beam of both, say at 60 A GeV, to extract the grey particle multiplicity distribution, for example. At $N_h \leq 1$ the number of events is 253. The priority of contribution in this sample is due to H nuclei. The rest is due to CNO then AgBr. Hence, the 105 events belonging to H nuclei are equivalent to 41.5% of 253 events. The matrix between N_h and N_g is entitled Matrix I shown in the appendix. Multiplying each cell of Matrix I by this percentage, as shown in Matrix II, the events due to H nuclei are obtained. The obtained N_g–distribution due to H nuclei is placed to the right of Matrix II. In Matrix III, the rest of the events, due to CNO and AgBr nuclei, is obtained and then placed in Matrix IV. The total number of events in this matrix is 519. Mentioned above that the no of events due to CNO nuclei is 344. This number is equivalent to 66.3% of 519 events. Applying this percentage on the Matrix IV as similar as the methods obeyed on

Matrix I, the CNO data can be obtained in Matrix V. The N_g-distribution due to CNO nuclei is placed to the right of Matrix V. In Matrix VI, the rest of events, due to AgBr nuclei, is obtained and then placed in Matrix IV. This matrix presents the AgBr data at $N_h \leq 8$. In order to extract the total sample of events due to AgBr nuclei, the Matrix IV can be extended to the whole ranges of N_h and N_g.

2.3. *Tracks identification*

The produced charged particles per event can be identified in the photographic nuclear emulsion according to their ionization characteristics.[1,2] They are classified into the below categories.

— The shower particles are mainly pions having K.E > 70 MeV and about 10% charged hadrons with K.E > 400 MeV. Their multiplicity is denoted n_s. The multiplicity of the forward and backward emitted shower particles are denoted n_s^f and n_s^b, respectively.
— The grey particles are mainly of knocked out target protons with $26 <$ K.E < 400 MeV. They have a little admixture of mesons. Their tracks have range > 3 mm and ionization, $1.4g_{\rm p} < g < 4.5g_{\rm p}$, where g is the measured grain density and $g_{\rm p}$ corresponds to the grain density of a minimum ionizing track. Their multiplicity is denoted as N_g. The multiplicities of the forward and backward emitted grey particles are denoted N_g^f and N_g^b, respectively.
— The black particles are evaporated target protons with K.E < 26 MeV. They have a short range in nuclear emulsion, ≤ 3 mm with $g > 4.5g_{\rm p}$. Their multiplicity is denoted N_b.
— The grey and black particles amount the group of heavily ionizing particles, denoted $N_h = N_g + N_b$.
— The projectile fragments are nuclear isotopes having $Z \geq 1$. They fly with the same speed of the projectile nucleus and are emitted in the forward narrow cone within $\theta_{\rm lab} \leq 3^\circ$.

3. Results

In the light of the fireball model,[32,33] the target and projectile nuclei make cylindrical cuts through each other in the overlapping region. This region encloses the participant nucleons from the projectile and target. Outside this region the nucleons are called spectators. The grey particle is expected to originate from the fireball and the black particle is evaporated from the spectator target. In what follows the black particle multiplicity is voted as centrality parameter.

3.1. *Multiplicity distribution*

In Fig. 1 through Fig. 4, the grey particle multiplicity is denoted N. This notation may indicate the grey particle emission in the 4π space, FHS, or BHS according

to the associated characters shown on the figures. The multiplicity distributions of the grey particle emitted in 60 A and 200 A GeV ^{16}O interactions with CNO emulsion nuclei are presented in Figs. 1 and 2, respectively at different centralities. Regarding the NLF, Figs. 1 and 2 indicate an agreement between the data of the

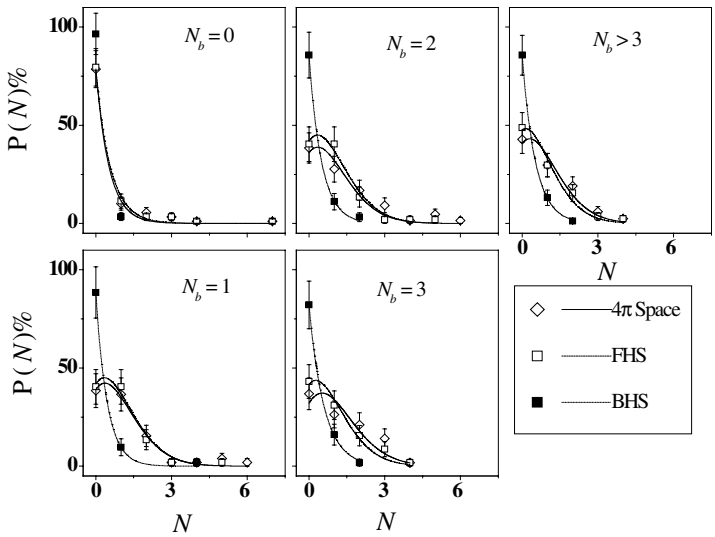

Fig. 1. The multiplicity distributions of the grey particle emitted in 60 A GeV ^{16}O interaction with CNO emulsion nuclei at different centralities, together with the fitting curves.

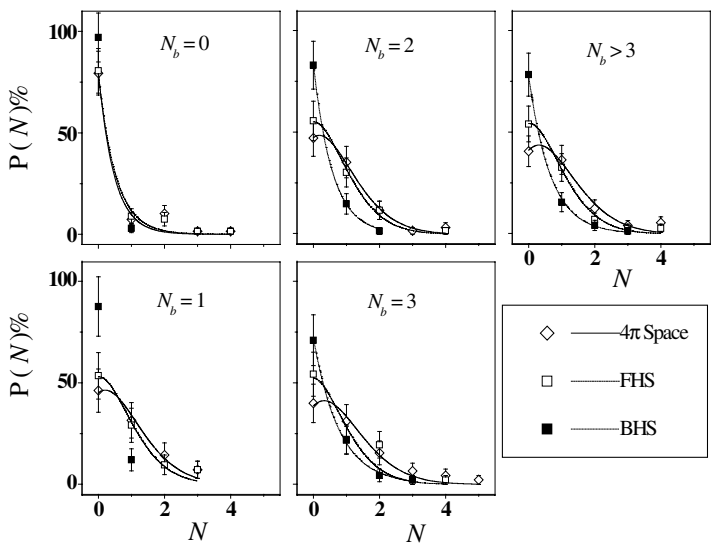

Fig. 2. The multiplicity distributions of the grey particle emitted in 200 A GeV ^{16}O interaction with CNO emulsion nuclei at different centralities, together with the fitting curves.

Table 3. The fit parameters of Eq. (1) for the grey particle emitted in the BHS through the present interactions with CNO emulsion nuclei.

E_{lab}	60 A GeV		200 A GeV	
Fit parameter	p	λ	p	λ
$N_b = 1$	88.46 ± 1.91	2.22 ± 0.20	—	—
$N_b = 2$	85.68 ± 1.68	2.00 ± 0.35	83.36 ± 0.97	1.74 ± 0.06
$N_b = 3$	82.19 ± 1.27	1.66 ± 0.08	71.80 ± 12.24	1.27 ± 0.22
$N_b > 3$	85.73 ± 0.78	1.90 ± 0.06	77.50 ± 10.40	1.50 ± 0.22

two energies at each centrality inset. The decay distributions are a characteristic of the grey particle emitted in the BHS at all centralities. Apart from the only two-point distributions at $N_b = 0$ or 1, the distributions in the BHS are fitted well by the exponential decay law of Eq. (1), where the fitting is presented in Fig. 1 by the smooth dotted curves. The fit parameter, p and λ, are listed in Table 3.

$$P(N)\% = pe^{-\lambda N}. \tag{1}$$

From Table 3 within experimental errors the fit parameters are similar at the two energies. The change of the fit parameters with the centrality is considerably negligible. Hence, one can say that the suggested system of the grey particle production in the BHS is independent on the energy and the voted centrality for ^{16}O+CNO collisions. At $N_b = 0$ the distributions of the grey particle emitted in the 4π space or FHS are approximated by exponential decay shapes fitted by Eq. (1). The corresponding fit parameters are listed in Table 4. This category may be referred to the most peripheral region. From Table 4, the fit parameters are nearly similar at the two energies. They are also the same irrespective of the emission direction in the 4π space or FHS within experimental errors. Hence, the fragmentation system at this centrality degree can work nearly to produce the forward emitted grey particle only. In comparison with the results of the backward emitted grey particles at all centralities, listed in Table 3, their values do not differ significantly from those of Table 4. Thus, one can say that the characteristics of the grey particle production system in the most peripheral region is as similar as those of the backward emitted one at all centralities of $^{16}\text{O} + \text{CNO}$ collisions.

At $N_b \geq 1$ the distributions are distinguished by shoulder-shaped curves. They are reproduced well by Poisson's shapes of Eq. (2). The Poisson's shapes are

Table 4. The fit parameters of Eq. (1) for the grey particle emitted in the 4π space or FHS through the present interactions with CNO emulsion nuclei at the most peripheral region, $N_b = 0$.

E_{lab}	60 A GeV		200 A GeV	
Fit parameter	p	λ	p	λ
4π Space	78.55 ± 2.72	1.92 ± 0.23	79.27 ± 5.55	2.11 ± 0.56
FHS	77.84 ± 9.42	1.74 ± 0.24	78.68 ± 10.93	1.91 ± 0.32

Table 5. The fit parameters of Eq. (2) for the grey particle emitted in the 4π space or FHS through the present interactions with CNO emulsion nuclei at different centralities.

E_{lab}	60 A GeV				200 A GeV			
Emission direction	4π space		FHS		4π space		FHS	
Fit parameter	α	β	α	β	α	β	α	β
$N_b = 1$	96.25 ± 4.53	0.90 ± 0.06	101.27 ± 5.56	0.88 ± 0.07	96.31 ± 6.78	0.76 ± 0.08	94.73 ± 7.34	0.58 ± 0.08
$N_b = 2$	88.03 ± 7.61	0.89 ± 0.10	94.17 ± 3.69	0.82 ± 0.05	98.98 ± 3.57	0.73 ± 0.04	98.88 ± 4.24	0.58 ± 0.04
$N_b = 3$	92.37 ± 13.98	1.06 ± 0.20	94.32 ± 6.68	0.82 ± 0.08	91.89 ± 5.32	0.86 ± 0.07	90.13 ± 14.01	0.54 ± 0.15
$N_b > 3$	94.81 ± 7.89	0.84 ± 0.10	95.12 ± 6.02	0.69 ± 0.07	96.79 ± 5.98	0.85 ± 0.07	97.82 ± 3.76	0.58 ± 0.04

presented in the figures by the solid and dashed smooth curves according to the emission in the 4π space and FHS, respectively. The parameters, α and β, are the normalization factor and $\langle N \rangle$ respectively. They are obtained by fitting the data and listed in Table 5.

$$P(N)\% = \alpha \frac{\beta^N}{N!} e^{-\beta}. \tag{2}$$

From Table 5, the change of the parameters w.r.t. the centrality is not significant. The predicted average multiplicities in the 4π space are nearly 0.9 and 0.8 according to 60 A and 200 A GeV, respectively. In the same respect, for FHS data, they are nearly 0.8 and 0.6. Therefore, the grey particle multiplicity is slightly steeper in the 4π space emission than FHS while it tends to be limited w.r.t. the centrality for ^{16}O+CNO collisions.

The multiplicity distributions of the grey particle emitted in 60 A and 200 A GeV ^{16}O interactions with AgBr emulsion nuclei are presented in Figs. 3 and 4, respectively at different centralities. From Fig. 3 in the most peripheral region at $N_b = 0$, the backward grey particle production is weak, where its distribution has two data points only. This is reflected on the forward emission distribution which is nearly superimposed on that of the 4π space emission. The two distributions, (of 4π space and FHS), are approximated by the exponential decay law of Eq. (1). The corresponding fit parameters are listed in Table 6.

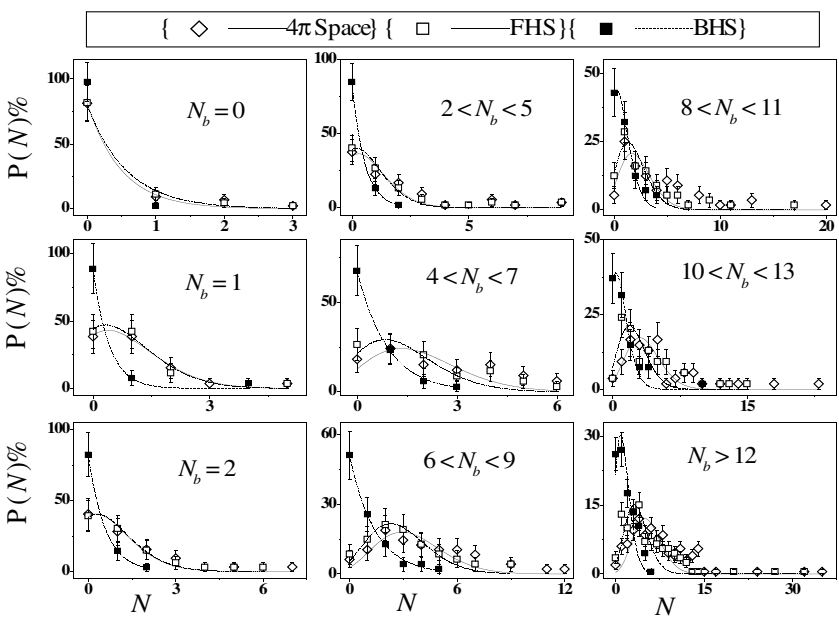

Fig. 3. The multiplicity distributions of the grey particle emitted in 60 A GeV ^{16}O interaction with AgBr emulsion nuclei at different centralities, together with the fitting curves.

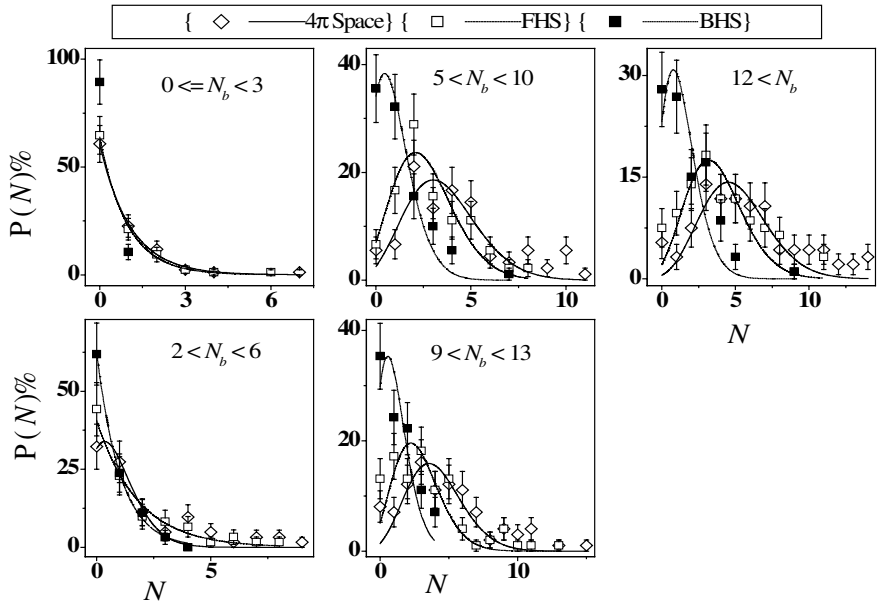

Fig. 4. The multiplicity distributions of the grey particle emitted in 200 A GeV ^{16}O interaction with AgBr emulsion nuclei at different centralities, together with the fitting curves.

Table 6. The fit parameters of Eq. (1) for the grey particle emitted in the 4π space or FHS through the present interactions with AgBr emulsion nuclei at the peripheral region.

E_{lab}	60 A GeV ($N_b = 0$)		200 A GeV ($0 \leq N_b \leq 2$)		200 A GeV ($3 \leq N_b \leq 5$)	
Fit parameter	p	λ	p	λ	p	λ
4π Space	81.29 ± 4.33	2.01 ± 0.39	60.51 ± 1.63	0.93 ± 0.05	—	—
FHS	79.94 ± 13.53	1.74 ± 0.34	63.83 ± 8.23	1.03 ± 0.13	40.59 ± 7.09	0.55 ± 0.09

The parameters are the same within experimental errors where the dominant emission is nearly in the FHS. The distributions of the grey particle emitted in the BHS are decay shaped in the centrality regions, $1 \leq N_b \leq 8$. They are approximated by the exponential decay law of Eq. (1). The corresponding fit parameters are listed in Table 7. The decay parameter in Table 7 seems nearly to decrease with the centrality. In the higher centrality regions, $N_b > 8$, the distributions are peaking shaped with narrow peaks. They are reproduced well by the Poisson's distributions of Eq. (2). The corresponding fit parameters are listed in Table 8. At centralities of $N_b > 0$, the grey particle distributions corresponding to the 4π space and FHS emissions are usually reproduced well by the Poisson's shapes of Eq. 2. The associated fit parameters are listed in Table 8. The evolution of these distributions peaking feature grows with centrality from the shoulder to normal shape where the distribution tends to be symmetric about the peak position. Similar characteristics are

Table 7. The fit parameters of Eq. (1) for the grey particle emitted in the BHS through the present interactions with AgBr emulsion nuclei.

$E_{\rm lab}$	60 A GeV		200 A GeV ($3 \leq N_b \leq 5$)	
Fit parameter	p	λ	p	λ
$N_b = 1$	88.45 ± 3.84	2.44 ± 0.50	62.58 ± 9.38	0.96 ± 0.15
$N_b = 2$	82.34 ± 0.30	1.76 ± 0.02		
$3 \leq N_b \leq 4$	84.90 ± 0.16	1.86 ± 0.01		
$5 \leq N_b \leq 6$	67.80 ± 1.37	1.10 ± 0.05		
$7 \leq N_b \leq 8$	51.15 ± 1.50	0.71 ± 0.03		

Table 8. The fit parameters of Eq. (2) for the grey particle emitted through the present interactions with AgBr emulsion nuclei at different centralities.

$E_{\rm lab} = 60$ A GeV	4π space		FHS		BHS	
Fit parameter	α	β	α	β	α	β
$N_b = 1$	99.60 ± 5.23	0.93 ± 0.07	104.67 ± 10.50	0.86 ± 0.12	—	—
$N_b = 2$	88.66 ± 8.22	0.83 ± 0.11	89.51 ± 4.99	0.85 ± 0.07	—	—
$3 \leq N_b \leq 4$	80.01 ± 9.77	0.83 ± 0.14	83.47 ± 5.46	0.76 ± 0.07	—	—
$5 \leq N_b \leq 6$	80.87 ± 15.20	1.85 ± 0.34	83.17 ± 12.06	1.37 ± 0.22	—	—
$7 \leq N_b \leq 8$	83.08 ± 9.22	3.45 ± 0.29	89.52 ± 6.20	2.81 ± 0.16	—	—
$9 \leq N_b \leq 10$	75.79 ± 11.29	2.20 ± 0.30	82.29 ± 0.06	1.82 ± 0.18	92.73 ± 6.60	0.79 ± 0.08
$11 \leq N_b \leq 12$	81.20 ± 0.30	3.54 ± 0.27	81.24 ± 12.11	2.39 ± 0.32	90.23 ± 7.13	0.92 ± 0.10
$N_b \geq 13$	71.15 ± 7.78	5.47 ± 0.39	72.46 ± 8.10	3.67 ± 0.30	86.97 ± 10.24	1.38 ± 0.18
$E_{\rm lab} = 200$ A GeV						
$3 \leq N_b \leq 5$	76.76 ± 7.69	0.89 ± 0.12	—	—	—	—
$6 \leq N_b \leq 9$	86.72 ± 9.49	3.53 ± 0.29	94.30 ± 8.58	2.60 ± 0.20	92.10 ± 6.52	0.99 ± 0.09
$10 \leq N_b \leq 12$	79.68 ± 8.23	4.06 ± 0.29	80.53 ± 9.85	2.76 ± 0.28	89.50 ± 14.97	1.10 ± 0.23
$N_b \geq 13$	79.47 ± 7.48	5.02 ± 0.29	83.53 ± 8.76	3.69 ± 0.28	85.92 ± 12.12	1.31 ± 0.21

nearly obtained at 200 A GeV from Fig. 4. From Table 8, the average multiplicities predicted by the Poisson's law increase with the centrality.

3.2. *Average multiplicity*

The average grey, $\langle N_g \rangle$, and black, $\langle N_b \rangle$, particles' multiplicities are listed in Table 9. The data of Table 9 are due to the present interactions in comparison with those of other labs and some theoretical simulations.

In Fig. 5, the average multiplicities, $\langle N_g \rangle$, $\langle N_g^f \rangle$, and $\langle N_g^b \rangle$ are correlated with the centrality for 60 A and 200 A GeV ^{16}O interactions with CNO emulsion nuclei. The symmetry extent between the FHS and BHS is examined by the (F/B) ratio. This ratio is defined as $(\langle N_g^f \rangle / \langle N_g^b \rangle)$, the so-called anisotropy factor. The change of (F/B) with centrality is displayed for the present interactions with CNO emulsion nuclei in Fig. 5. From Fig. 5, in general, the data fluctuate nearly along the centrality range, except the deviation at $N_{\rm b} = 0$ and $N_{\rm b} > 6$.

Table 9. The average grey and black particles' multiplicities of the present interactions in comparison with these of other experiments.

E_{lab}	$\langle N_g \rangle$	$\langle N_b \rangle$	Emulsion type or simulation code	Ref.
60 A GeV	2.65 ± 0.12	6.10 ± 0.30	FUJI	Present work
200 A GeV	2.24 ± 0.10	5.37 ± 0.18	ILFORD G5	
60 A GeV	2.16 ± 0.15	4.91 ± 0.34	FUJI	34
200 A GeV	2.03 ± 0.11	5.39 ± 0.29	ILFORD G5	34
60 A GeV	2.64	—	VENUS Model	34
200 A GeV	1.97	—	VENUS Model	34
200 A GeV	3.90 ± 0.20	4.80 ± 0.20	BR–2	26
200 A GeV	4.30 ± 0.20	4.00 ± 0.20	BR–2	35
200 A GeV	1.80	0.14	FRITIOF Model (Version 1.7)	35
3.7 A GeV	6.40 ± 0.50	3.90 ± 0.20	NIKFI–BR2	36
200 A GeV	5.10 ± 0.30	4.10 ± 0.20	NIKFI–BR2	36
3.7 A GeV	4.55	—	NIKFI–BR2	37
3.7 A GeV	5.67	—	NIKFI–BR2	27

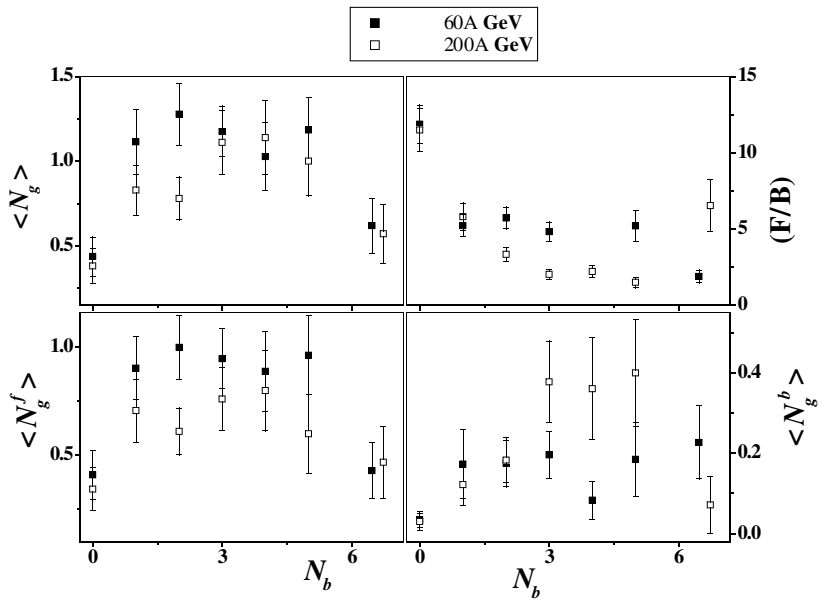

Fig. 5. The dependence of the grey particle average multiplicities on the centrality through 60 A and 200 A GeV ^{16}O interactions with CNO emulsion nuclei.

In Fig. 6, the average multiplicities and (F/B) ratios are correlated with the centrality for the present 60 A and 200 A GeV ^{16}O interactions with AgBr emulsion nuclei. From Fig. 6 the average multiplicities depend strongly by a linear correlation on the centrality. The linear fit parameters are listed in Table 10. The (F/B) ratio fluctuates along the centrality range, except the peripheral region up to $N_b \sim 3$

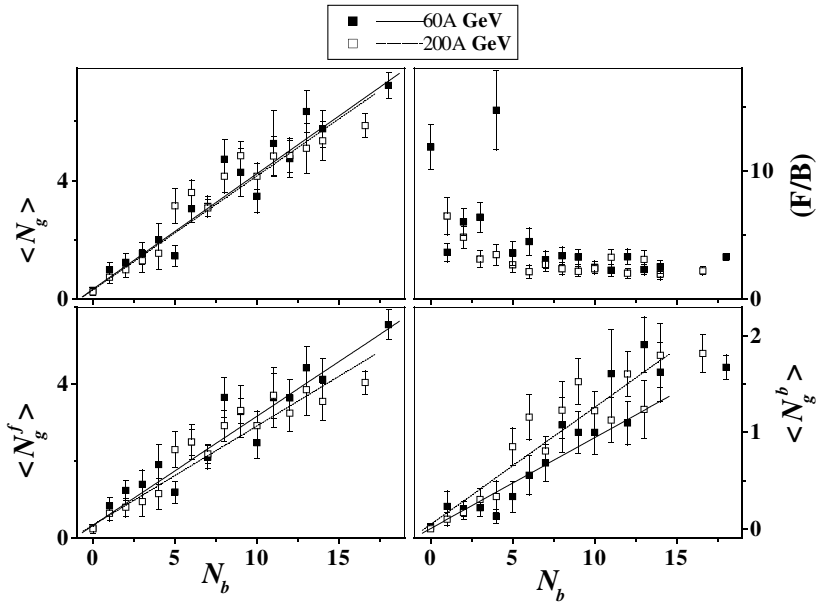

Fig. 6. The dependence of the grey particle average multiplicities on the centrality through 60 A and 200 A GeV ^{16}O interactions with AgBr emulsion nuclei, together with the fitting curves.

Table 10. The fit parameters of the straight lines of Fig. 6.

$E_{\rm lab}$	60 A GeV		200 A GeV	
Fit parameters	Intercept	Slope	Intercept	Slope
4π space	0.35 ± 0.10	0.39 ± 0.02	0.33 ± 0.11	0.38 ± 0.02
FHS	0.34 ± 0.09	0.28 ± 0.02	0.35 ± 0.10	0.26 ± 0.02
BHS	0	0.09 ± 0.01	0.05 ± 0.11	0.12 ± 0.01

beyond which, it tends nearly to constant value ~ 3. Over a wide range of projectile size, $A_{\rm Proj} = 1$ to 207, and energy, $E_{\rm lab} = 2.1$ A–200 A GeV, (F/B) is found nearly 3 at average impact parameter.[24]

The multiplicity dispersion, D, is defined by Eq. (3), where N is the multiplicity. The dispersion is denoted D_g, D_g^f and D_g^b according to the multiplicities, $\langle N_g \rangle$, $\langle N_g^f \rangle$ and $\langle N_g^b \rangle$, respectively. In Fig. 7, the dispersion variation with the centrality for the present interactions is shown.

$$D = \sqrt{\langle N^2 \rangle - \langle N \rangle^2}. \tag{3}$$

From Fig. 7 for CNO targets, the dispersions fluctuate nearly along the centrality range. For AgBr targets, the dispersions increase linearly with the centrality. The increase is presented in the figure by the straight line segments. The fit parameters of these lines are listed in Table 11.

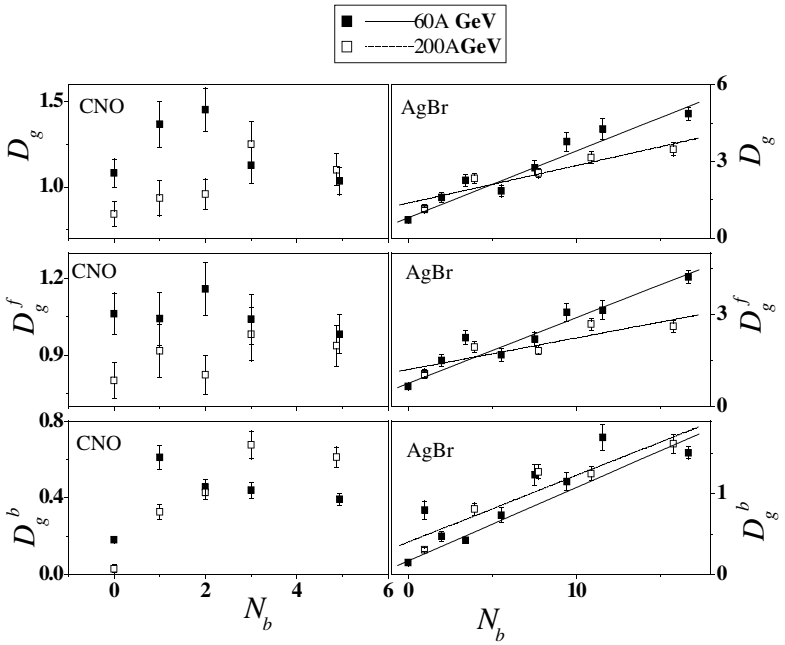

Fig. 7. The dispersion at different centralities of 60 A and 200 A GeV ^{16}O interactions with emulsion nuclei, together with the fitting lines.

Table 11. The fit parameters of the straight lines of Fig. 7.

E_{lab}	60 A GeV		200 A GeV	
Fit parameters	Intercept	Slope	Intercept	Slope
4π space	0.79 ± 0.10	0.26 ± 0.02	1.36 ± 0.29	0.15 ± 0.03
FHS	0.75 ± 0.10	0.21 ± 0.02	1.20 ± 0.29	0.10 ± 0.03
BHS	0.17 ± 0.04	0.09 ± 0.01	0.40 ± 0.15	0.08 ± 0.02

4. Discussion

In the present experiment, the NLF hypothesis is regarded. Therefore, the energy is not an effective parameter. On the basis of a wide range of thermodynamic models, Gyulassy and Kauffmann show that the Poisson distribution can predict the emitted particle multiplicity in the central collision regions.[38] In a heavy–ion collision no deviation is found also from a Poisson distribution in the central collision regions.[39] On the other hand, statistically the binomial distribution is the base of the probability function. This distribution can converge towards the Poisson's distribution. The Poisson's distribution itself can convert from the decay shape to the normal shape, the so-called Gaussian. This evolution is associated with different stages of the system properties, as temperature, centralities, size, etc. Therefore, one suggests that the decay shape implies a single source contribution to the system. The multi source system is indicated by the peaking-shaped distribution, which is a super-position

of single sources. In this species, the peaking distribution shape changes from the shoulder shape to the bell shape according to the contribution of each source to the system. The bell shape, as Gaussian, is associated with the isotropy of state where the contributions of all sources are equivalent. In the framework of the intranuclear cascade model,[40–43] the grey particle mainly can result from the binary NN collisions and/or intranuclear cascading. According to the fireball model, explained by Westfall *et al.*,[32] the binary NN collisions and intranuclear cascading can occur between the participant nucleons in the overlapping between the colliding nuclei. Therefore, the grey particle has to be sourced mainly from the participant matter where the fireball is formed. The temperature of the grey particle production system is predicted in the framework of the modified statistical model as ∼60 MeV.[7,8] At Bevalac energies, $E_{\text{lab}} \sim 0.1$ A to 2 A GeV, the fireball temperatures range from 30 MeV to 125 MeV.[44] Hence, the temperature of the grey particle production system is sourced from a fireball formation. Kinematically, its emission has to be in the FHS. It is pointed out in the introduction that the grey particle emission in the BHS, beyond the kinematic limits, can be due to two mechanisms.[12] The first is a pion production followed by its absorption on two target nucleons resulting in two back-to-back nucleons emission. The second is a production of Δ which is absorbed, subsequently, by a target nucleon, $\Delta N \rightarrow NN$, resulting in two protons emission of 180° correlation angle nearly. Consequently, a half part of these production systems are enclosed also in the forward emitted particle multiplicity. Thus, the grey particles are multisource production system. Moreover, the distribution main features are indicator to the system properties.

For the light target size, CNO, the multiplicity distribution features indicate the following:

— At the most peripheral region, $N_b = 0$, the decay feature is dominant in the 4π space, FHS, or BHS emissions. Therefore in the most peripheral region, the grey particle production system is resulted from a single source. This source is reasonable to be due to the binary NN collision only.
— At $N_b > 0$, the Poisson's shape continues with insignificant changes along the whole centrality range in the FHS. Therefore, another source accompanied by the intranuclear cascading works beside that of the binary NN collisions with unequal contributions. The centralities, associated with this light target size, are insufficient to exhibit the isotropy of state for the two sources contributions.
— A similar decay feature continues at all centralities for the emission in the BHS. Therefore, the centralities, associated with this light target size, cannot permit the activation of more than one source.

For the heavy target size, AgBr, the multiplicity distribution features indicate the following:

— Not only at the most peripheral region but also up to $N_b \sim 2$, the decay feature is a dominant characteristic in the 4π space or FHS emissions. Therefore in the

peripheral regions, the grey particle production system is resulted from a single source. This source is reasonable to be due to the binary NN collision only.

— At higher centralities, the Poisson's shape continues with observed changes along the whole centrality range in the FHS. Therefore, another source accompanied by the intranuclear cascading works beside that of the binary NN collisions. At $N_b \geq 6$ the Poisson's shape seems to be symmetric about the peak, regardless the low probable long multiplicity tail. Therefore at these centralities the two sources can have equivalent contributions where the isotropy of state exists.

— At centralities lower than $N_b \sim 6-8$, the decay feature is a dominant characteristic, where a single source contribution is suggested in the BHS. At the higher centralities, the Poisson's shoulder shape continues with insignificant change. Therefore, the two suggested mechanisms of the backward production[12] can be considered with unequal contributions.

As known, the grey particle is sourced from the participant target nuclear matter in the overlap region between the two colliding nuclei. In the framework of the cascade evaporation model and its modification, reviewed in Refs. 45 and 46, the spectator target part is excited during the binary NN collisions, parton–nucleon collisions, and/or intranuclear cascading. The excitation may occur also as a result of pion absorption at the surface of the overlap region by the spectator part. The black particle is evaporated from the spectator part during a long time comparing with the parton formation time. Therefore the size of the spectator part is related with the system overlapping, and consequently the grey particle multiplicity is related with the black particle multiplicity. Geometrically the overlapping size increases on the expense of the spectator part or in other words the grey particle production is anti-correlated with the black particle production. While the provided excitation increases the spectator part size has to be too sufficient to produce black particle. Therefore, the black particle production can go along to the grey particle one, provided that there is a sufficient spectator size. In ^{16}O+CNO collisions the system is nearly symmetric. Hence, at the most central collisions the target and projectile nuclei are completely occulted by each other. The grey particle production increases with the centrality in equivalent proportion up to the halves of the two colliding nuclei overlap. At this centrality stage the grey particle production can have a plateau effect, after which it decreases. The CNO events separation on the basis of N_h restrictions can show that for large N_b value N_g is forced to be small. At $N_b = 0$ the deviation may be due to admixture of interactions with H nuclei. The dependence of the average multiplicities on the centrality, in Fig. 5, seems to be compatible with this description. At the most central region of ^{16}O+AgBr collisions, the projectile nucleus dives completely in the target nucleus. An adequate spectator size exits at all centralities, where the grey particle production goes along the black particle production. Hence the linearity of the correlations, in Fig. 6, is reasonable to be the always trend.

5. Conclusions

Measurements of the grey particle multiplicity in 60 A and 200 A GeV ^{16}O interactions with emulsion nuclei provide insight into the earlier stage of the target fragmentation. The multiplicity is determined in terms of the energy, emission direction, target size and centrality. In the literature, the centrality is investigated at ^{16}O+CNO and ^{16}O+AgBr collision systems.

— Regarding the NLF, the grey particle multiplicity characteristics are similar at the two energies.
— In ^{16}O+CNO collisions, the decay shape is the usual characteristic feature of the multiplicity distribution at all centralities for the emission in the, BHS. The emission in the FHS at the most peripheral region is characterized also by the decay shaped distribution. At the other centralities the Poisson's shape is a characteristic in the FHS. However, the variation of the distribution shapes w.r.t. the centrality is insignificant. The average multiplicities and dispersion always fluctuate along the centrality range. This implies a constant variation w.r.t. the centrality. Hence for the light target size this production system seems to be limited w.r.t. the impact parameter.
— In ^{16}O+AgBr collisions, the decay shape is the usual characteristic feature at centralities up to $N_b \sim 8$ for the emission in the BHS. At $N_b > 8$, the Poisson's shape is the characteristic with narrow peaks. The distributions are always Poisson's shape for the emission in the FHS, but only the peripheral region is characterized by the decay shape. Almost at $N_b > 8$, the Poisson's shapes tend to be symmetric about the peak to match the Gaussian shapes. The average multiplicities, predicted by the Poisson's law, increase with the centrality. The average multiplicities depend strongly on the centrality by linear functions. The anisotropy factor is nearly 3 at $N_b > 2$. This observed value seems to be limited over the all collision systems, energies, and nearly impact parameters. The dispersion is correlated with the centrality by a linear relation. This implies a strong change with the centrality. Hence for the heavy target size this production system is not limited w.r.t. the impact parameter.
— It is suggested that the grey particle is a multisource production system. The sources may be associated with the binary NN Collisions, the parton–nucleon collisions, and the intranuclear cascading. Kinematically the produced particle, due to these sources, is emitted in the FHS. The results indicate that the majority of the grey particles are produced due to these sources. There are other two suggested sources. They are the pion production followed by its absorption by two target nucleons which are emitted back-to-back; and Δ production followed by its absorption by one target nucleon then two nucleons are emitted back-to-back. Hence, the grey particle originated from these sources is emitted isotropically in the FHS as well as in the BHS. The sensibility to the centrality or target size is different from one source to other. All of these sources are insensitive to the energy or projectile size. Therefore, some of these sources can

work at any impact parameter or target size while others are not able. This is reflected on the characteristic features of the multiplicity distributions. In this species, the decay shape indicates a source singularity while the peaking shape is a super-position of a multi-source system. The isotropy of state can exist when the contributions of the all sources become equivalent.

— The selectivity of the black particle multiplicity as a centrality parameter is successful in the collision systems associated with heavy target sizes. When the target size is light another parameter is recommended to be selected.

Acknowledgment

We are pleased to acknowledge the kind help of the CERN authorities for providing us the photographic emulsion plates irradiated by 60 A and 200 A GeV ^{16}O at SPS, EMU03 experiment.

Appendix

Matrix I

	N_h	
N_g	0	1
0	179	52
1		22

Matrix II N_g-Distribution

	N_h			
N_g	0	1	N_g	Frequency
0	$(179 \times 41.5/100) \sim 74$	$(52 \times 41.5/100) \sim 22$	0	$(74 + 22) = 96$
1		$(22 \times 41.5/100) \sim 9$	1	9

Matrix III

	N_h	
N_g	0	1
0	(179–74) = 105	(52–22) = 30
1		(22–9) = 13

Matrix IV

	N_h								
N_g	0	1	2	3	4	5	6	7	8
0	105	30	38	32	26	12	7	4	5
1		13	29	27	23	13	14	9	2
2			8	12	16	18	9	10	5
3				4	2	9	12	4	4
4					1	1	1	1	3
5							3	4	0
6								1	1
7								1	

Matrix V N_g-Distribution

	N_h										
N_g	0	1	2	3	4	5	6	7	8	N_g	Frequency
0	70	20	25	21	17	8	5	3	3	0	172
1		9	19	18	15	9	9	6	1	1	87
2			5	8	11	12	6	7	3	2	52
3				3	1	6	8	3	3	3	24
4					1	1	1	1	2	4	6
5							2	3	0	5	5
6								1	1	6	2
7								1		7	1

Matrix VI

	N_h								
N_g	0	1	2	3	4	5	6	7	8
0	35	10	13	11	9	4	2	1	2
1		4	10	9	8	4	5	3	1
2			3	4	5	6	3	3	2
3				1	1	3	4	1	1
4							0	0	1
5							1	1	

References

1. C. F. Powell, F. H. Fowler and D. H. Perkins, *The Study of Elementary Particles by the Photographic Method* (Pergamon Press, London; New York, Paris, Los Angles, 1958), p. 474.
2. H. Barkas, *Nuclear Research Emulsion: Technique and Theory*, Vol. 1 (Academic Press, Cambridge 1963).
3. M. S. El–Nagdy, *Phys. Rev. C* **47** (1993) 346.
4. EMU01 Collab. (I. Otterlund *et al.*), *Phys. Scr.* **T32** (1990) 168.
5. EMU01 Collab. (M. I. Adamovich *et al.*), *Phys. Rev. Lett.* **62** (1989) 2801.
6. H. H. Heckman, H. J. Crawford, D. E. Greiner, P. J. Lindstrom and W. Wilson Lance, *Phys. Rev. C* **17** (1978) 1651.
7. A. Abdelsalam, *Phys. Scr.* **47** (1993) 505.
8. A. Abdelsalam, E. A. Shaat, Z. Abou–Moussa, B. M. Badawy and Z. S. Mater, *Radiat. Phys. Chem.* **91** (2013) 1.
9. L. S. Schroeder, Lawrence Berkeley Laboratory Preprint–LBL 11102, Invited Talk Presented at the 1980 Institute for Nuclear Studies, Kikuchi Summer School on Nuclear Physics at High Energies, Fuji–Yoshida, Japan 1–4 (July 1980).
10. L. S. Schroeder, *Nucl. Instrum. and Methods* **162** (1979) 395.
11. S. A. Chessin, J. V. Geaga, J. Y. Grossiord, J. W. Harris, D. L. Hendrie, R. Treuhaft and Bibber K Van, *Phys. Rev. Lett.* **43** (1979) 1787.
12. J. W. Harris, *Proc.* of The Workshop on Nuclear Dynamics 80, Lawrence Berkeley Laboratory, California (March 17–21, 1980).
13. J. Benecke, T. T. Chou, C. N. Yang and E. Yen, *Phys. Rev.* **188** (1969) 2159.
14. J. V. Geaga, S. A. Chessin, J. Y. Grossiord, J. W. Harris, D. L. Hendrie, L. S. Schroeder, R. N. Treuhaft and Bibber K Van, *Phys. Rev. Lett.* **45** (1980) 1993.
15. A. Abdelsalam, N. Metwalli, S. Kamel, M. Aboullela, B. M. Badawy and N. Abdallah, *Can. J. Phys.* **91** (2013) 438.
16. M. S. El–Nagdy, A. Abdelsalam, Z. Abou–Moussa and B. M. Badawy, *Can. J. Phys.* **91** (2013) 737.
17. A. Abdelsalam, E. A. Shaat, Z. Abou–Moussa, B. M. Badawy and Z. S. Mater, *Chin. Phys. C* **37** (2013) 084001.
18. P. Brogueira, J. Dias de Deus and C. Pajares, *Phys. Rev. C* **75** (2007) 054908.
19. PHOBOS Collab. (B. B. Back *et al.*), *Phys. Rev. Lett.* **91** (2003) 052303.
20. BRAHMS Collab. (I. G. Bearden *et al.*), *Phys. Lett. B* **523** (2001) 227.
21. BRAHMS Collab. (I. G. Bearden *et al.*), *Phys. Rev. Lett.* **88** (2002) 202301.
22. PHOBOS Collab. (B. B. Back *et al.*), *Nucl. Phys. A* **757** (2005) 28.
23. PHOBOS Collab. (B. B. Back *et al.*), *Nucl. Phys. A* **715** (2003) 490c.
24. A. Abdelsalam, M. S. El–Nagdy, N. Rashed, B. M. Badawy, W. Osman and M. Fayed, *Can. J. Phys.* **93** (2015) 361.
25. Shmakov A. Yu and V. V. Uzhinskii, *Comput. Phys. Comm.* **54** (1989) 125.
26. KLM Collab. A. Dąbrowska, R. Hołyński, A. Jurak, A. Olszewski, M. Szarska, A. Trzupek, B. Wilczyńska, H. Wilczyński, W. Wolter, B. Wosiek, K. Woźniak, M. L. Cherry, W. V. Jones, K. Sengupta, J. P. Wefel, P. S. Freier and C. J. Waddington, *Phys. Rev. D* **47** (1993) 1751.
27. D.-H. Zhang, H.-H. Zhao, F. Liu, C.-L. He, H.-M. Jia, X.-Q. Li, Z.-Y. Li and J.-S. Li, *Chin. Phys.* **15** (2006) 1987.
28. J. R. Florian, M. Y. Lee, J. J. Lord, J. W. Martin, R. J. Wilkes, R. E. Gibbs and L. D. Kirkpatrick, *Phys. Rev. D* **13** (1976) 558.

29. A. Abdelsalam, *Inelastic Interactions of p, d,* ^{4}He *and* ^{12}C *Projectiles with Light (CNO) and Heavy (AgBr) Nuclei at* 4.5 *GeV/c per Nucleon*, JINR Report (Dubna), E1–81–623 (1981).
30. E. O. Abdrahmanov *et al.*, *Z. Phys. C* **5** (1980) 1.
31. EMU01 Collab. (M. I. Adamovich *et al.*), *Substructual Dependence of the Multiparticle Production in Relativistic Heavy-Ion Interaction*, Lund University Report, Sweden, LUIP 8904, May (1989).
32. G. D. Westfall, J. Gosset, P. J. Johansen, A. M. Poskanzer, W. G. Meyer, H. H. Gutbrod, A. Sandoval and R. Stock, *Phys. Rev. Lett.* **37** (1976) 1202.
33. J. Gosset, H. H. Gutbrod, W. G. Meyer, A. M. APoskanzer, A. Sandoval, R. Stock and G. D. Westfall, *Phys. Rev. C* **16** (1977) 629.
34. P. L. Jain, G. Singh and K. Sengupta, *Phys. Rev. C* **43** (1991) R2027(R).
35. EMU01 Collab. (M. I. Adamovich *et al.*), *Phys. Lett. B* **234** (1990) 180.
36. L. Fu–Hu, *Chin. J. Phys.* **40** (2002) 159.
37. S. M. Abd–Elhalim and A. Callet, *Chaos Solitons and Fractals*, **18** (2003) 115.
38. M. Gyulassy and S. K. Kauffmann, *Phys. Rev. Lett.* **40** (1978) 298.
39. M.-C. Lemaire *et al.*, *Phys. Rev. C* **43** (1991) 2711.
40. M. K. Hegab and J. Hüfner, *Nucl. Phys. A* **384** (1982) 353.
41. V. I. Bubnov *et al.*, *Z. Phys. A* **302** (1981) 133.
42. M. K. Hegab and J. Hüfner, *Phys. Lett. B* **105** (1981) 103.
43. M. Tosson, O. M. Osman, M. M. Osman and M. K. Hegab, *Z. Phys. A* **347** (1994) 247.
44. R. Stock, *Phys. Rep.* **135** (1986), 259.
45. EMU01 Collab. (M. I. Adamovich *et al.*), *Z. Phys. A* **358** (1997) 337.
46. A.-W. Khaled, *Phys. Rev. C* **59** (1999) 2792.